A comparison between sea-bottom gravity and satellite altimeter-derived gravity in coastal environments: A case study of the Gulf of Manfredonia (SW Adriatic Sea)

L. S. Zampa[1,2], E. Lodolo[1], N. Creati[1], M. Busetti[1], G. Madrussani[1], E. Forlin[1], A. Camerlenghi[1]

[1]National Institute of Oceanography and Applied Geophysics - OGS - Italy
[2]Department of Mathematics and Geosciences - University of Trieste - Italy

Key Points:

- Comparison between sea-bottom and satellite altimeter-derived gravity allowed to estimate the noise effects in altimeter data, near-shore.
- The high-resolution sea-bottom gravity available along the Italian coasts detects effects of sources not seen by satellite altimeter data.
- Combined analysis of satellite altimeter and sea-bottom gravity gives a complete view on the offshore continuation of near-shore structures.

Corresponding author: Luigi Sante Zampa, `lzampa@inogs.it`

Abstract

The marine gravity field derived from satellite-altimetry is generally biased, in coastal areas, by signals back-scattered from the nearby land. As a result, the derived gravity anomalies are mostly unreliable for geophysical and geological interpretations of near-shore environments.

To quantify the errors generated by the land-reflected reflections and to verify the goodness of the geologic models inferred from gravity, we compared two different altimetry models with sea-bottom gravity measurements acquired along the Italian coasts. We focused on the Gulf of Manfredonia, in the SE sector of the Adriatic Sea, where: (i) two different sea-bottom gravity surveys have been conducted over the years, (ii) the bathymetry is particularly flat, and (iii) seismic data revealed a prominent carbonate ridge covered by hundreds meters of Oligocene-Quaternary sediments. Gravity field derivatives have been used to enhance both (i) deep geological contacts and (ii) coastal noise. The analyses outlined a ringing-noise compromising the altimeter signals up to 17 km from coasts. Differences between observed data and gravity calculated from a geological model constrained by seismic data, showed that all investigated datasets register approximately the same patterns, associated with the Gondola Fault Zone.

This study showed the potential for implementing gravity anomalies derived from satellite-altimetry with high resolution near-shore data, such as the sea-bottom gravity network available around the Italian coasts. This type of analysis may find future applications to better investigate connections between marine and inland geology in transitional areas.

Plain Language Summary

We present a comparative analysis between two types of gravity-data used in geophysical studies: satellite altimeter-derived gravity and sea-bottom gravity. It is largely known that the quality of satellite altimetry data in the vicinity of the coast is hindered by signals reflected from nearby lands. We show how this problem may affect the interpretation of gravity anomalies, and how it could be solved by integrating altimetry-derived gravity with high-resolution marine gravity-networks available in the proximity of coasts. We chose as a test area the Gulf of Manfredonia, in the South Adriatic coast of Italy, which hosts a major tectonic feature i.e. the Gondola Fault Zone. The fault zone is not clearly expressed at the sea-floor, which is generally flat, but it dislocates carbonate rocks located hundreds meters below the sediments, and in doing so it creates lateral density contrasts prone to be detected by gravity data.

Keywords

Sea-bottom gravity, Satellite altimeter-derived gravity, Coastal noise, ISVD, Tilt

1 Introduction

It is largely known that the quality of sea-surface height measurements from satellite radar altimetry in coastal regions is hindered by the noisier radar returns from the generally rougher coastal sea states and simultaneous returns from reflective land and inland water (Andersen & Knudsen, 2000). Therefore, satellite altimeter-derived gravity in the vicinity of lands is inevitably contaminated by "non-gravity signals".

Some solutions have been found to improve the altimeter-derived results using the waveform tracking technique, which reprocesses the waveform data through a "coastal retracking system", as performed along the Australian coastal regions (Deng & Featherstone, 2006). The resolution of these methods has been continuously increasing in the last decades, also thanks to newly available and more accurate radar data. Moreover, radar altimetry has the advantage of a near-global coverage and almost homogeneous

error characteristics away from the coasts (Fu & Cazenave, 2000; Green et al., 2019). When comparative data acquired independently and with different techniques are available, such as marine geophysical measurements, it is possible to provide a more exhaustive and quantitative assessment of the satellite altimetry errors. From the early 50s to the late 80s the Osservatorio Geofisico Sperimentale (OGS) of Trieste (Italy) performed several gravimetric surveys along the Italian coasts using sea-bottom gravity meters (Ciani et al., 1960; C. Morelli, 1966; Gantar, 1983), during which thousands of data-points have been recorded (Figure 1).

In this study, we investigate the compatibility of (i) sea-bottom gravity with (ii) satellite altimeter-derived gravity, using both the DTU13 (Andersen et al., 2014) and the S&S (Sandwell et al., 2014) datasets and provide a quantitative evaluation of the differences between the two gravity data-types. To circumscribe the effectiveness of such comparison (satellite-derived gravity vs. sea-bottom gravity), this study focuses on a relatively small coastal area in the SE Adtriatic Sea, The Gulf of Manfredonia, where two different sets of sea-bottom gravity data have been acquired over the years.

The choice for this study area is motivated essentially by the following reasons: (i) it is a very flat sector of the coastal region, where a thick, ellipsoidal-shaped sedimentary basin has been identified with seismic reflection profiles; (ii) a dense grid of gravity measurements acquired at the sea-bottom is available; (iii) seismic profiles show the presence of significant geological discontinuities propagating from inland (Gargano Peninsula) towards the offshore (Gulf of Manfredonia), and thus prone to be detectable by the gravity data; (iv) it represents an ideal case in which the flat sea-floor does not mimic the trend of the rock-basement below the sea-floor sediments, which instead can be easily imaged by gravity anomalies.

The relative sea-bottom measures were connected with the national absolute gravity network, which was also upgraded over the years, causing systematic bias between data-points taken in different periods over the same areas. All measurements were concentrated near the coasts, since: (i) the vessel position was easier to triangulate from land, and (ii) the proximity of docking harbours guaranteed a fast and frequent connection with land-based gravity stations, thereby reducing large residual drift errors in the final absolute gravity values.

These data were never coupled with sea-surface gravity, which acquisition started in the 60s (C. Morelli, 1966). Despite the acquisition disadvantages, sea-bottom gravity is more sensitive to sub-bottom density variations and less affected by levelling errors than sea-surface gravity (Talwani et al., 1966; Ballu et al., 1998; Fairhead, 2016). All the gravity dataset have been preliminary corrected for the same reference model: the Bouguer anomaly of sea-bottom data takes into account the free-water gradient and gravity effects of topographic and water masses above and below the sea-bottom station, while the Bouguer anomaly of altimeter-derived gravity just considers topographic and water effects of masses above and below the sea surface.

We used the Integrated Second Vertical Derivative (ISVD) and the Tilt functions to enhance the noise effects and, at the same time, the gravity signals from the edges of causative sources. These functions have been compared with the same results obtained from a forward gravity-model derived from seismic-reflection data. This helped to investigate the relative sensitivity of each dataset to the gravity effect of known sources, and it also provided a better understanding of where and which dataset was more repairable for the interpretation of gravity anomalies.

The results may find useful application in studying continuity and configuration of geological contacts, marked by density contrasts from inland to the offshore coastal areas, and the method here described could be easily implemented to significantly reduce errors caused by coastal noise in satellite altimeter-derived gravity, in similar coastal regions where sea-bottom gravity measurements are available.

1.1 Geological setting

The Gulf of Manfredonia is located in the SW sector of the Adriatic Sea. It is limited to the north by the Gargano Peninsula and to the west by the northern part of the Puglia region (i.e., the northern sector of the Salento). Within the gulf, the bathymetry reaches the maximum water-depths of ∼90 m, with a smooth sea floor surface, without showing any relevant morphological features. The lithostratigraphy of the area, to a depth of ∼2.5 km have been divided in four main units (D. Morelli, 2002; Volpi et al., 2015): (i) the Plio-Quaternary sandy and clayey sediments, (ii) the Upper Oligocene–Miocene argillaceous and marly turbidites, (iii) the middle Liassic-Paleogene pelagic limestones and marls, and (iv) the upper Triassic-lower Liassic evaporitic, dolomitic and shallow water limestones. The two lowest units (iii and iv), which we generally called "Jurassic-Paleagene carbonate succession", form the solid bedrock. The bedrock is covered by unconsolidated or partially consolidated siliciclastic sediments up to depths of ∼1500 meters in the deepest basin (Figure 2b).

Seismic studies conducted since the 70s have revealed the presence of an important structural element beneath the sedimentary cover, striking broadly W-E, known as the Gondola Fault Zone. The Gondola Fault Zone includes several E–W and NW-SE trending fault segments that define an elongated, buried structural high called "Gondola ridge" (Colantoni et al., 1990; de Alteriis & Aiello, 1993; de Alteriis, 1995), which extends ∼70 km across the shelf without producing significant morphologies at the sea-floor along most of its extension (Ridente & Trincardi, 2006). Conversely, a tectonic-related relief visibly affects the sea-floor morphology down-slope, along the ∼50 km-long NW-SE branches of the Gondola Fault Zone (Tramontana et al., 1995; de Alteriis, 1995). The Gondola Fault zone has been related to a Cenozoic reactivation of pre-existing faults (Finetti, 1983; Tramontana et al., 1995). Quaternary activity has been documented by deformation of Middle Pleistocene sediment. The overall geometry of the Gondola Fault Zone suggests a significant right-lateral component of motion (Ridente et al., 2008).

The Gondola fault system continues onshore with the Mattinata Fault that cuts through the Gargano Promontory (Figure 2a), which is an E–W elongated relief (maximum elevation ∼1000 m) along the flexural bulge of the Adriatic foreland (Ridente et al., 2008). The Gondola and Mattinata fault zones can be traced for a total length of at least 180 km (Di Bucci et al., 2006), and belong to the ∼15 km wide corridor of fault system that from the Adriatic Sea reach the core of the Apennines (Ridente et al., 2008). The Mattinata Fault is considered as a poly-phased belt, subjected to an intense deformation acting since Mesozoic times and formed by several fault splays (Billi et al. (2007), and references therein). However, seismic data have shown that the Mattinata Fault is neither in direct continuity nor perfectly aligned with the Gondola Fault Zone, showing an under-lap of ∼20 km and right-stepping of ∼5 km (Ridente et al., 2008).

2 Data

In this study, we calculate and compare gravity anomalies covering the Gulf of Manfredonia using four different datasets: two satellite altimeter-derived gravity dataset, i.e. the DTU13 (Andersen et al., 2013, 2014, 2015) and the S&S (Sandwell et al., 2014), and two sea-bottom gravity datasets, i.e. OGS60 (Ciani et al., 1960) and OGS83 (Gantar, 1983). To constrain the forward gravity model, we used the geological model produced by Volpi et al. (2015).The model is based on the interpretation of multichannel seismic profiles made available through the project ViDEPI (Visibility of Petroleum Exploration Data in Italy, www.videpi.com, managed by the Italian Ministry of Economic Development), and released in SEG-Y format by the web portal SNAP "Seismic data Network Access Point", maneged by the Istituto Nazionale di Oceanografia e di Geofisica Sperimentale (Diviacco, 2018).

2.1 Satellite altimeter derived gravity

Satellite altimeter-derived gravity comes from measurements of the Sea Surface Heights (SSH), obtained by radar satellites orbiting at ∼800 km from the Earth surface. A microwave pulse emitted from the satellite antenna is reflected back by a portion of the sea surface (footprint), which position is mapped relatively to the reference ellipsoid. This allows a full reconstruction of the SSH over almost the entire globe. After correcting the SSH for time-dependent components, residual orbital errors, and the Mean Dynamic Topography (a quasi-stationary component of SSH), the result is a static realization of the marine geoid (Andersen et al., 2010). The mathematical relation between geoid undulations (N) and the Free-air anomaly (Fa) is given by the Bruns formula:

$$Fa = -g^s_{th}\frac{\partial N}{\partial r} - \frac{2}{R}N g^s_{th} \tag{1}$$

where, g^s_{th} is the theoretical gravity (spherical approximation), N is the geoid undulation and R is the mean Earth radius.

There are two methods available to compute the vertical geoid gradient $\frac{\partial N}{\partial r}$, from altimetry data: (i) the "geoid-to-gravity" and (ii) the "slope-to-gravity" (Fairhead, 2016).

2.1.1 DTU13

The DTU13 dataset was obtained with the "geoid-to-gravity" method, developed by Geotechnical University of Denmark (Fairhead, 2016). In this approach, the vertical derivative is computed starting from 2-D regular grids of the geoid. The geoid grids result from spatial interpolation of radar data, crossover adjusted, and corrected for time-variable and stationary components of the SSH, i.e. all those components not directly related to the gravity field of the solid-Earth (Andersen et al., 2010, 2014).

The derivation is performed using the Fast Fourier Transform (FFT), after having removed the effect of the EGM2008 spherical harmonic model up to degree and order 2160 (Pavlis et al., 2012), i.e. wavelengths ≤20 km (Barthelmes, 2009). Then, the removed harmonic components are added back on the final result (remove-restore technique).

The resulting Free-air anomaly is available in a grid format, with a sampling-step of 1 arc-min (Figure 3a). However, the real maximum resolution is limited by the along-track spacing of observations, which is around 6÷7 km, and by the systematic use of a Wiener low-pass filter with cut-off wavelengths ranging between 5 and 16 km (Andersen & Knudsen, 1998; Andersen et al., 2010). As a result, the shortest reliable wavelength hovered around a full-waveforms of ∼13 km (Andersen, 2013; Fairhead, 2016).

The DTU13 is associated with an interpolation error file (Figure 3b), showing uncertainties on the vertical component of the Mean Sea Surface grids (MSS_{err}) which is defined in units of meters (Andersen & Knudsen, 2009). This error shows the quality of gridded data points and it can be used to roughly identify the transition between land and ocean (Andersen et al., 2008). However, it may underestimate the real uncertainties, also because it does not include errors from EGM2008 model (Andersen & Knudsen, 2009).

The relation between geoid and gravity (eq. 1), gives ∼1 mGal amplitude for a sea surface slope of 7 mm/7 km (Sandwell et al., 2013), i.e. ∼1.4 mGal/cm when considering horizontal distances of ∼7 km (i.e. full-waveforms of ∼14 km). This simple equivalence can be used to convert roughly the MSS_{err} grid values into mGal units.

2.1.2 S&S

The S&S dataset used the "slope-to-gravity method", which is based on the same remove-restore principle of DTU13, but in this case the derivatives are directly computed from along-track signals, instead of 2-D grids. Resulting slopes are interpolated and con-

volved to obtain grids of W-E, S-N horizontal gravity gradients, and these gradients are finally combined through the Laplace equation to obtain the vertical gravity component (Sandwell, 1992; Fairhead, 2016).

The S&S Free-air anomaly is available in grid format with a sampling-step of 1 arc-min (Figure 3c), and it is also associated to an error-grid which defines its uncertainty (Figure 3d). In this case, the error refers directly to the gravity anomaly, i.e. it is expressed in mGal units, and it shows the RMS difference between (i) the slope of individual altimeter profiles and (ii) the averaged grid product of W-E and S-N slope (Sandwell & Smith, 2009; Sandwell et al., 2014).

Tanks to the direct computation of gradients from along-track signals, the S&S model may preserve high frequencies better than the DTU13, albeit it may also amplify residual noises, i.e. non modelled disturbing components (waves, tides, currents) or renaming scattered spikes, especially in coastal regions.

2.1.3 Coastal noise

Errors of satellite altimeter data generally increase close to the coast, where the radar footprint covers also part of the inland together with the sea surface (Dawson et al., 2015). Reflections from onshore areas generate large amplitude noise covering signals reflected by the sea surface (Figure 3b,d). The exact distance from the coastlines where these contaminations may occur is not easy to estimate, since it depends on a complicated combination of different factors, e.g. the angle between orbital tracks and shoreline, topographic and bathymetric gradients, local bathymetry, and local tides. This makes coastal noise a site-dependent problem mostly.

Even if in the last decades (i) Interferometric Synthetic Aperture Radar (e.g. CryoSat-2 mission), (ii) more accurate global gravity models (e.g. EGM2008) and (ii) more sophisticated tracking techniques allowed to consistently reduce such noise, signal accuracy up to $\sim 7 \div 14$ km from coats may be compromised (Deng & Featherstone, 2006; Andersen & Knudsen, 2009; Sandwell & Smith, 2009; Dawson et al., 2015)

For this specific reasons, interpretations of altimeter-derived gravity in coastal regions must be carefully evaluated and preferably integrated with ship-borne/air-borne gravity or other types of geophysical data.

2.2 Sea bottom gravity data

2.2.1 OGS60

OGS60 is part of a dataset recorded during a seven-year mission (1953 - 1960) to extend offshore the Italian land-based gravity network (RFI) and to create the firsts gravity maps of the Italian seas (Ciani et al., 1960). Gravity data were measured using a Western sea-bottom relative meter, with a nominal accuracy of 0.05 mGal. Station depths were measured by echo-sounders (Atlas-WerKe) and coordinates calculated using optical and/or radar instruments pointing to coastal marks or reflective buoys. Planar coordinates precision decreases with increasing distances from the coast: from a minimum of ± 50 m inshore, to a maximum of ± 200 m at ~ 120 km from the coast, or even up to ± 600 m when reflective buoys were not available. OGS60 stations are not regularly distributed, i.e. station spacing increases towards the offshore, from a minimum of ~ 1.6 km to a maximum of ~ 10 km at $\sim 60 \div 70$ km from the coast (Figure 3e).

2.2.2 OGS83

OGS83 data were collected in 1982, under the commission of the “Agip Mineraria” company, as part of a 98-days marine gravity survey to create high-resolution gravity maps of the Adriatic coast, from Ancona to Ortona (”northern zone”) and from Manfredonia to Brindisi (”southern zone”). Gravity differences were measured with a LaCoste&Romberg sea-bottom relative meter (mod. 19 G), which has also a nominal accuracy of 0.05 mGal

(Gantar, 1983). Stations depth was measured by both echo-sounders (Honeywell ELAC, mod. LA2721A) and pressure meters, giving a final combined accuracy of ±0.5 m. Horizontal coordinates were calculated by means of radar trilateration from the coast (Motorola System), with a nominal precision of ±3 m ±0.01*distance[km]. The OGS83 stations are distributed on a nearly regular grid, up to ∼10 km from the coast, with an almost constant separation distance of ∼1±0.2 km (Figure 3e).

3 Methods

The computation of gravity anomalies from sea-bottom data (OGS60 and OGS83), slightly differs from the procedure normally used with sea-surface data (e.g. DTU13 and S&S). A correct comparison can only be achieved when both data-types are corrected for the same disturbing effects, i.e. all the gravity signals not related to the sub-bottom target sources (Ballu et al., 1998). To achieve this condition, we first calculate the Free-water anomaly, Fw, for the sea bottom gravity data:

$$Fw = g_{obs} - (g_{th} + fwc) \tag{2}$$

where, g_{obs} is the observed gravity and fwc is the Free-water correction.

Then, we calculate the Bouguer anomaly of both altimeter-derived gravity and sea-bottom gravity (Ba_{sat} and Ba_{sb}), by using two different solutions based on a common computational scheme to derive the total topographic effect (Te_{sat} and Te_{sb}):

$$Ba_{sat} = Fa – Te_{sat} \tag{3}$$

$$Ba_{sb} = Fw – Te_{sb} \tag{4}$$

where, Fa is the free-air of satellite-altimetry datasets (eq. 1).

After computing the Bouguer anomaly, the OGS83 and OGS60 stations have been merged into a unique dataset, i.e. OGS. The validity of this merging-operation is supported by the statistics of data differences, when comparing the two datasets within the near-shore overlapping area. Most of differences range between ±1.2 mGal, with an average bias that is negligible when compared to satellite altimeter errors (Table 1). This finding ensures a precision higher than 1 mGal for sea-bottom gravity, since the repetition of measurements in two different periods over the same area, give an average discrepancy of just ∼0.58 mGal (RMS).

The Bouguer anomaly of sea-bottom data, as a final step, should have been upward-continued from the drape sea-floor surface to a constant mean sea level, in order to have all datasets at the same distance from the causative sources (Ballu et al., 1998). However, being the average sea-floor at ∼50 m depth (mean vertical step) and gravity stations separated by non-less than 1 km (smallest horizontal step), the upward-continuation amplitude would have been lower than 1 mGal and likely affected by numerical noise. Therefore, we decide to skip this last processing-step.

3.1 Theoretical gravity (g_{th})

The theoretical gravity, g_{th}, was calculated using the WGS84 ellipsoid as a reference model (Decker, 1986), i.e. the same used for satellite altimetry. The WGS84 model includes all the mass of the atmosphere above the reference surface within the total mass of the solid Earth. Then, effects of the outer masses must be removed from the theoretical gravity, since the net gravitational force exerted by the atmospheric shell on any point inside is close to zero (Hinze et al., 2005):

$$g_{th}(\lambda) = \frac{978032.67714\left(1 + 0.001931851386 sin^2\lambda\right)}{\left(1 - 0.00669437999013 sin^2\lambda\right)^{1/2}} - g_{atm} \tag{5}$$

where, λ is the geographic latitude and g_{atm} is the value for atmospheric correction at the sea level, i.e. 0.87 mGal.

3.2 Free-water anomaly (Fw)

The theoretical gravity of stations located below the water masses was corrected for the relative depth of each measurement point, using the free-water correction fwc (Stacey & Tuck, 1981; Luyendyk, 1984; Dubois & Deplus, 1989; Hildebrand et al., 1990; Ballu et al., 1998):

$$\begin{aligned} fwc(h) &\simeq \frac{\partial(g^s_{th} - g_{shell})}{\partial r} h \\ &\simeq -\frac{2\, g^s_{th}}{R^2}\, h \;+\; 4\pi G \rho_w h \\ &\simeq -0.222\, h \end{aligned} \tag{6}$$

where, h is the station depth ($h \leq 0$), r is the radial distance to the center of the Earth, ρ_w is the water density (1030 kgm^{-}3), g_{shell} is the downward attraction of an homogeneous spherical shell and G is gravitational constant ($6.67 * 10^{-11}$ m^{3}s^{-2}/kg).

The free-water correction is similar in principle to the atmospheric correction: the water layer overlying the measurement point approximates the most outer homogeneous spherical shell of the reference model, which has a null gravity effect on the inner region. Then, the total downward gravitational attraction of the theoretical model (i) slightly decreases with depth because of the lack of mass contribution from the thickening outer shell. This effect is opposite to the (ii) larger increment in the gravitational attraction due to the closer proximity with the Earth-mass centre. The combination of both effects is a slight decreasing of the vertical gravity gradient by a quantity $\sim$ equal to the gravitational attraction of the water shell (eq. 8).

The homogenous-spherical shell approximation holds, if (i) the density does not change drastically within the water column and if (ii) the effect of Earth curvature is negligible (Bullard, 1936). The study area fills both conditions, since it is less than 200 km large and the water layer is on average $\sim$50 m thick. Otherwise, the ellipsoidal-shell approximation and water-density profiles should have been included in the computation (Stacey & Tuck, 1981).

3.3 Topographic effect (Te)

The gravity effects of topographic and water masses in the Bouguer anomaly (eq. 3, eq. 4), was computed differently in the case of sea-bottom (OGS60, OGS83) and sea-surface gravity (DTU13, S&S), since sea-bottom stations are located at different distances from the surrounding masses than sea-surface measurements.

In both cases the adopted computational scheme, considers separately the effect of (i) a high-resolution DTBM (Digital Topographic-Bathymetric Model) with a grid-step of 100 m, extended for 9 km from the computational point, and (ii) the effect of a low-resolution DTBM, with 3 km grid-step which extends for 159 km from the limits of the high resolution area.

The DTBM model is created from a mash-up of SRTM and EMODnet data (Farr & Kobrick, 2000; Consortium et al., 2018), composed by 3-D prisms. The gravity effect of each prism is calculated through the python library Harmonica (Uieda et al., 2020), which makes use of the analytical solution proposed by Nagy et al. (2000), having the advantage of being valid on any point, either outside or inside the element (Nagy et al., 2002; Fukushima, 2019).

3.3.1 Topographic effect at the sea-surface (Te_{sat})

When computing the Bouguer anomaly, if the measurement point lies on the sea surface (as for altimeter-derived gravity), the reference model must be corrected for effects of crustal masses above it and water masses below it (Figure 4a,b).

Supposing a constant density for both Earth-crust and sea water (ρ_c=2670 kg/m^3 and ρ_w=1030 kg/m^3), a first approximation of the topographic effect Te is given by (i) the vertical upward attraction of outside crustal masses, decreasing the theoretical gravity value (negative effect) and (ii) the drop in gravitational attraction due to the presence of water masses instead of crust in marine areas (negative effect). This approximation may vary locally, because of inland depressions (continental areas below the reference surface), or inland water masses (e.g. large lakes or lagoons).

The solution (eq. 10) is identical for measurement points above the reference surface (e.g. land-based stations or air-born measurements), with the difference that the attraction of topographic masses may be both positive and negative, depending on the high of the point compared to the surrounding topography.

$$\begin{cases} Zone(A): \ g_e(h, 0, \rho_c) & if \ h > 0 \\ Zone(B): \ g_e(0, h, \rho_w - \rho_c) & if \ h < 0 \end{cases}$$
$$Te_{sat} = \sum_A g_e(h_t, h_b, \rho) + \sum_B g_e(h_t, h_b, \rho) \tag{7}$$

Here, g_e is the gravitational attraction of a prism, with h_t and h_b being respectively the top and the bottom height of the element, and h the height given by the DTBM model.

3.3.2 Topographic effect at the sea-bottom (Te_{sb})

The gravitational effect of the reference model g_{th}, after the Free-water correction lacks the attraction of all masses above the computational point, which are not homogeneously distributed within a spherical shell (as assumed in eq. 8), but rather unevenly distributed between crust, water and atmosphere (Figure 4c,d).

Then, the gravity effect of all the known masses heterogeneously distributed above the computational point must be added as an upward attraction to the theoretical gravity (negative effect). The remaining effects of masses below the computational point ($Zone(C)$, Figure 4d) should be treated as for the case of sea-surface stations, i.e. by removing the effect of crust and adding back the effect of water (eq. 11).

The problem is solved by dividing the DTBM model in three zones (Gantar, 1983; Nowell, 1999):

$$\begin{cases} Zone(A): \ g_e(h, h_s, \rho_c) & if \ h > 0 \\ Zone(B): \ g_e(0, h, \rho_w) + g_e(h, h_s, \rho_c) & if \ h_s < h < 0 \\ Zone(C): \ g_e(0, h_s, \rho_w) + g_e(h_s, h, \rho_w - \rho_c) & if \ h < h_s < 0 \end{cases}$$
$$Te_{sb} = \sum_A g_e(h_t, h_b, \rho) + \sum_B g_e(h_t, h_b, \rho) + \sum_C g_e(h_t, h_b, \rho) \tag{8}$$

where, hs is the depth of the computational point (i.e. negative height).

3.4 Field derivatives

Gravity field derivatives are commonly used in geophysical studies to enhanced lateral density contrasts in-depth (Fedi & Florio, 2001; Aydogan, 2011; de Lerma et al., 2015). The multi-scale derivative has already proven useful in identifying the offshore continuation of the Mattinata Fault system (i.e. the "Gondola ridge"), on larger scale regional analysis (Fedi et al., 2005). In this study, we use the Integrated Second Vertical Deriva-

tive (ISVD) and the Tilt derivative (Miller & Singh, 1994; Fedi & Florio, 2001; Fedi, 2002), for a qualitative evaluation of the sensitivity to lateral density contrast, of each different gravity datasets (DTU, S&S, OGS). The ISVD was calculated in three steps (Fedi & Florio, 2001): (i) integrating the gravity anomaly grid in the frequency domain, (ii) computing the second-order horizontal derivatives in space domain using a 2-D convolution and (iii) calculating the first-order vertical derivative combining the results from the previous step through the Laplace equation.

The Tilt derivative is simply the angle given by the ratio between the ISVD and the first-order horizontal gravity gradient, which is also computed through a spatial-domain convolution:

$$Tilt = atan\left(\frac{ISVD}{\sqrt{\frac{\partial g}{\partial x} + \frac{\partial g}{\partial y}}}\right) \tag{9}$$

where, g is the gravity anomaly and $\sqrt{\frac{\partial g}{\partial x} + \frac{\partial g}{\partial y}}$ is the total horizontal gradient.

The calculated functions have been qualitatively evaluated by a direct comparison with the forward gravity model derived from the geologic model which includes the interface between the Oligocene-Quaternary sediments and the underlying carbonate platform, as taken from the previous work of Volpi et al. (2015), in which depths were derived from a 2-D inversion of multichannel seismic profiles constrained by well-logs data. The gravity effect of the seismic interface is computed using the Parker method in FFT domain (Parker, 1973):

$$\Delta\ \mathrm{g}\,(x,y) = FFT^{-1}\left\{-2\pi G\Delta\rho e^{-h_0|\vec{K}|}\sum_{n=1}^{\infty}\frac{\left|\vec{K}\right|^{n-1}}{n!}FFT\left[h\,(x,y)^n\right]\right\} \tag{10}$$

where, Δg is the gravity effect of the 2D interpreted seismic layers, depth-converted, h is the depth of the layer, $\Delta\rho$ is density contrast between the two layers forming the interface, h_0 is the mean depth of the interface, $\vec{K}$ is the wavenumber.

A first-order polynomial surface was removed from the Bouguer anomaly before computing the derivatives. The linear trend should well approximate the effects of deep sources, since, in the Italian territory, both the Moho and the crystalline basement have wavelengths larger than 100 km (Corrado et al., 1981), and this study area is less than 90 km extended.

The Tilt function allowed to map the edges of gravity sources from the residual gravity field. Lines approximating edges were outlined through a maximum detection algorithm build using a 3 x 3 km moving window operator (Blakely & Simpson, 1986). The operator slides on the cosine of the Tilt, also known as Theta derivative. The Theta derivative is always positive and locates its maxima where the Tilt is equal to zero, which correspond approximately to the position of sub-surface lateral discontinuities (Wijns et al., 2005; Fairhead, 2016). The ridge axis of the Gondola system was calculated with the same solution but using directly the Tilt instead of the Theta function, since the Tilt has the advantage of showing maximum values directly over the top-centre of the causative sources. The detected edges have been divided in two sets: (i) a first set containing lines correlating with faults interpretation based on seismic profiles or with visible changes in the trend of carbonate platform (verified edges) and (ii) a second set containing lines only registered by gravity (inferred edges). The "gravity edges" combine both the results from OGS data, within a coastal strip ∼17 km large, and the S&S data in the remaining areas.

4 Results and Discussion

The Bouguer anomaly values follow approximately a bimodal distribution (figure 5a). The first mode, located at ∼60 mGal, is representative of the area south of the Gondola fault system. The second mode, located at ∼75 mGal accounts for values in the northern sector, with relatively higher positivity than the southern. The differences between southern and northern sectors are mainly related to the abrupt discontinuity at the Gondola Fault Zone. This discontinuity cuts the main Bouguer trend, which represent a long wavelength regional-signal of the Bouguer (i.e. wavelengths ≥200 km), SW-NE oriented. Regional signal are likely related to crustal discontinuities below the top of the carbonate layer, e.g. the crystalline basement and/or the Moho (Corrado et al., 1981). Then, the presence of a nearly vertical step of ∼30 mGal breaking the continuity of the main gravity trend, may suggests that the origin of the Gondola System is deeper than the base of the Jurassic carbonates, which hovered around depths of 2÷3 km (Volpi et al., 2015).

The relative minimum of ∼-30 mGal, near the western coast extends for ∼30 km in the SW-NE direction, ∼50 km in the NW-SE direction, and it shows similar amplitude and shape in all the studied datasets (DTU, S&S, and OGS). With the information gathered from seismic reflection data, it is possible to assert that part of this gravity minimum is related to a localized sedimentary ∼1500 m deep.

The Bouguer anomaly values of DTU shows approximately the same statistics and similar spatial distribution of S&S (Table 2 and figure 5b,c). However, S&S model has (i) higher amplitudes and (ii) shorter wavelengths than DTU, as shown by the data distribution and by the map of data differences (figure 5a,e). The S&S data register short-wavelengths anomalies near the SE coast, ∼6 km width, which occurs as a sort of "ringing effect", reasonably caused by the radar signals reflected from adjacent land areas, i.e. coastal noise (figure 5c). This noise compromises the S&S grid up to a maximum distance from the coast of ∼17 km, calculated as the normal distance between the coastline and the first zero contour in the ISVD grid of S&S data, over the largest anomalous "ring effect" in the SE coastal-sector (figure 6h).

Differences between OGS and satellite altimeter datasets (DTU and S&S) show values greater than 15 mGal in the vicinity of the NW coast (i.e. the Gargano Promontory). Here, high positive differences correlate with high topographic gradients (figure 5e,f,g). However, this coastal area is also poorly covered by sea-bottom stations (more than 6 km apart from each other), which means differences may also be caused by interpolation artefacts, other than coastal noise. The RMS difference of DTU and S&S compared to OGS data (Table 2), is approximately within the estimated errors of satellite altimeter datasets (Andersen et al., 2014; Sandwell et al., 2014). Nevertheless, the maximum and minimum differences are greater than 20 mGal, meaning that there are local errors a few tens of mGals higher than the predicted uncertainties, if considering sea-bottom gravity as a correct reference.

After removing a first-order linear trend, the residual anomaly (figure 6a,d,g) should correlate with the carbonate basement, i.e. it should respond mainly to the density contrast between carbonate rocks and the overlying terrigenous sequence (Corrado et al., 1981; Rapolla, 1986; Fedi & Rapolla, 1993). This hypothesis is partially confirmed by the forward gravity model based on seismic reflection data, which shows patterns similar to the observed residual gravity. However amplitudes of residual gravity onto the Gondola ridge are almost ∼10 mGal higher than the calculated gravity, which may reinforce the hypothesis of a deeper origin than the Jurassic sequence, for the base of this Gondola System.

The residual gravity, the ISVD, and the Tilt maps (figure 6) give further evidence that S&S contains higher frequencies than DTU: it has both (i) the highest ringing noise near the coast, and (ii) the sharpest gravity gradient in correspondence with the Gondola ridge, as highlighted by the forward gravity model. The ISVD of S&S data correlates positively with the ridge axes. In addition, the dataset resolution allows to follow the slight change in the axis orientation from NW-SE to E-W, which is less clear in both

the DTU and OGS data. This confirms that S&S, among the investigated datasets, is the most accurate away from the coast, and at the same time the noisiest in near-shore areas. On the other hand, the OGS data are the most reliable in the in the vicinity of coasts, since here they count on a nearly regular distribution of stations, separated by distances of ∼1 km, and also they do not register any evident systematic bias between data acquired in subsequent surveys (Figure 3e and Table 1).

The ISVD map of OGS data shows local relative minima close to the coast, with sizes ranging from 5 to 6 km (figure 6b). Each of these minima is covered by more than three gravity stations, and they are not related to any local structural discontinuity shown by seismic reflection profiles on the top of carbonate layer, which appears to be relatively flat in this sector. Excluding the presence of localized deeper sources and/or measurement biases, these small gradient changes may be related to localized variations within the Pliocene and Pleistocene sediments (D. Morelli, 2002; Volpi et al., 2015). As described in the geological setting, at least two different sedimentary units have been recognized from the interpretation of seismic profiles (Figure 2b): the upper unit is composed by Plio-Quaternary siliciclastic sediments, which we supposed less dense and less compacted than the lower Oligocene-Miocene unit composed by silico-clastic and calcareo-clastic turbidites (Volpi et al., 2015). The normal superposition of these units has been supposed locally modified by tectono-eustatic processes (D. Morelli, 2002), and probably by different sedimentary river inputs and erosion mechanisms, leading to lateral depositional transitions (heteropy of facies). The ISDV map (figure 6b) shows that one of the relative minima is located just in front of the mouth of the Ofanto river (figure 7e), the largest river in the Puglia region that transports and deposits a considerable amount of sediments to the sea (Mastronuzzi et al., 2002). This hypothesis, if confirmed, could be an important prove of the capabilities of the Italian sea-bottom gravity network, to distinguish even small density variations within sedimentary bodies, which may turns extremely useful in the absence of seismic profiles acquired in the immediate vicinity of the coast.

The ISVD and the Tilt derivatives enhance lateral density transitions: in both functions, the zero value marks approximately the edges of causative sources, i.e. lateral discontinuities of subsurface interfaces. The Tilt, unlike ISVD, is normalized between $\pm\pi/2$ and it tend to saturates faster over the top of those bodies with relatively high densities. This property makes the Tilt particularly useful when it comes to outline the planar shape of the carbonate platform, as imaged by gravity grids (figure 7).

All the investigated datasets are in good agreement when tracking the position of the SW edge of the Gondola system. However, they do not have enough resolution and perhaps accuracy to outline correctly the NE side of the ridge. On this side, the half-wavelength of the graben is shorter and smoother than on the southern side, where it is ∼10 km wide. In this area, even the OGS sea-bottom stations are also separated by distances ranging from 6 to 10 km (Figure 3e). As a result, the observed gravity does not fit with the forward model as on the West side of the Gondola ridge; instead it appears smoother and stretched towards NE (figure 7c).

The gravity edges, south of the Gondola ridge, correspond approximately to the Jurassic faults interpreted from seismic (D. Morelli, 2002). Also, the central axis of the ridge, derived from gravity, correlates well with the pre-existing seismic interpretation (D. Morelli, 2002; Volpi et al., 2015). This confirms that part of the information contained in both sea-bottom and satellite-altimetry gravity consists of a 3-D sub-surface fault network (Fedi & Florio, 2001; FitzGerald & Milligan, 2013; Fairhead, 2016). The remaining signals are associated with lateral density contrasts not necessarily related to the sub-vertical steps in the rock basement (figure 7e). Some of the "inferred edges" extracted from S&S data emerge on the NE and NW side of the map, where the rock/sediment transition is more gradual and the gravity edges outline the middle of the tilted sides of the interface, rather than its upper edge. Other inferred edges, derived from OGS data instead, contour local minima near the coast. Some of them correlate with SW-NE oriented Paleogene faults, cutting the southern shoreline sector (figure 7e). These lineaments are Dinaric transfer faults, which reactivate an older NE-SW Jurassic horst-graben sys-

tem (D. Morelli, 2002). The reactivation dislocates the Oligocene-Miocene deposits, forming a lateral transition between them and the upper and less-dense sedimentary unit.

5 Conclusions

In this study sea-bottom gravity measurements (OGS) have been compared with sea-surface satellite altimeter-derived gravity (DTU and S&S), in the Gulf of Manfredonia.

All the investigated gravity data-types, once corrected for effects of the free-water gradient and topographic/water masses, show statistical compatibility and spatial correlation in the main patterns imaged by the gravity anomalies. All datasets show the same negative anomaly associated with a ∼1500 m deep basin located immediately to the south of the Gondola Fault Zone. The residual gravity, ISVD and Tilt functions register the effects of the central carbonate ridge as outlined by the seismic reflection profiles.

A comparison with the forward gravity model obtained from seismic interpretation, showed that the S&S dataset allows a more accurate identification of the sediment/rock lateral transition, when compared to the other gravity datasets (i.e. DTU and OGS). However, S&S is deeply compromised by coastal noise in the first 17 km from the shoreline, where the interpretation of residual gravity is largely inconsistent. The DTU dataset shows a lower high-frequency content than S&S data, despite being less noisy near-shore.

The combined interpretation of OGS sea-bottom and S&S data allowed to confidently trace the edges of the carbonate platform, both near and far from the coast, as imaged by gravity. Part of the gravity edges correlates with faults detected by seismic profiles within the Gondola Fault Zone. Other edges mark the smooth transition between rock and sediments, rather than abrupt discontinuities generated by faults. Some edges, detected only by sea-bottom gravity near the eastern coast, outline shallow anomalies with low amplitudes, which could be related to relatively small density contrasts in the river deposits and/or differential sediment compaction. In a few cases, these near-shore edges seems also partially related to lateral discontinuities, SW-NE oriented, as identified by seismic data. This finding shows how the high-resolution sea-bottom gravity network around the Italian coasts contains information about sub-surface geological structures, not fully detectable by nor satellite-altimetry or available seismic data.

The comparative analysis described here the effectiveness of coupling information from both sea-bottom and satellite-altimeter derived gravity to reduce uncertainties of altimeter signals in localized coastal areas. In particular, the results helped to outline and better image geological structures propagating from inland towards the offshore areas of the Salento region, with more accurate results than when using just a single gravity or seismic datasets.

Acknowledgments

All grid files and maps were created using Generic Mapping Tools (GMT) version 6.1.1.

The multichannel seismic-reflection data comes from the project ViDEPI (Visibility of Petroleum Exploration Data in Italy), managed by the Italian Ministry of Economic Development, and made available in SEG-Y format on the platform SNAP "Seismic Data Network Access Point" managed by the Istituto Nazionale di Oceanografia e Geofisica Sperimentale (Diviacco, 2018).

The S&S dataset is available through Sandwell et al. (2014), at https://www.earthbyte.org/new-global-marine-gravity-model-sandwell-et-al-2014.

The DTU13 dataset is available through Andersen et al. (2013), at https://ftp.space.dtu.dk.

The OGS sea-bottom gravity dataset is part of the OGS gravity database (Ciani et al., 1960; C. Morelli, 1966).

The DTBM is a mash-up of SRTM and EMODnet data. The SRTM product is released by the National Geospatial Intelligence Agency (NASA) and downloaded from the USGS EROS Data Center, courtesy of the U.S. Geological Survey. The EMODnet product is provided by the EMODnet Bathymetry Consortium (2018): EMODnet Digital Bathymetry (DTM).

For the topographic corrections we used the python library Harmonica, which is part of the project Fatiando a Terra (Uieda et al., 2020), available at https://www.fatiando.org.

References

Andersen, O. B. (2013). Marine gravity and geoid from satellite altimetry. In *Geoid determination* (pp. 401–451). Springer.

Andersen, O. B., & Knudsen, P. (1998). Global marine gravity field from the ERS-1 and Geosat geodetic mission altimetry. *Journal of Geophysical Research: Oceans*, *103*(C4), 8129–8137. doi: 10.1029/97JC02198

Andersen, O. B., & Knudsen, P. (2000). The role of satellite altimetry in gravity field modelling in coastal areas. *Physics and Chemistry of the Earth, Part A: Solid Earth and Geodesy*, *25*(1), 17–24. doi: 10.1016/S1464-1895(00)00004-1

Andersen, O. B., & Knudsen, P. (2009). The DNSC08 mean sea surface and mean dynamic topography. *Journal of Geophysical Research: Solid Earth*(114), C11. doi: 10.1029/2008JC005179

Andersen, O. B., Knudsen, P., & Am Berry, P. (2010). The DNSC08GRA global marine gravity field from double retracked satellite altimetry. *Journal of Geodesy*, *84*(3), 191–199. doi: 10.1007/s00190-009-0355-9

Andersen, O. B., Knudsen, P., Berry, P., Freeman, J., Pavlis, N., & Kenyon, S. (2008). The DNSC08 ocean wide altimetry derived gravity field: EGU Meeting Programme. *Abstract EGU2008-A-07163, G1-1MO1O-003*.

Andersen, O. B., Knudsen, P., Kenyon, S., Factor, J., & Holmes, S. (2013). The dtu13 global marine gravity field—first evaluation. In *Ocean surface topography science team meeting, boulder, colorado.*

Andersen, O. B., Knudsen, P., Kenyon, S., & Holmes, S. (2014). Global and arctic marine gravity field from recent satellite altimetry (DTU13). In *76th eage conference and exhibition 2014* (Vol. 2014, pp. 1–5). doi: 10.3997/2214-4609.20140897

Andersen, O. B., Knudsen, P., & Stenseng, L. (2015). The dtu13 mss (mean sea surface) and mdt (mean dynamic topography) from 20 years of satellite altimetry. In *Igfs 2014* (pp. 111–121). Springer.

Aydogan, D. (2011). Extraction of lineaments from gravity anomaly maps using the gradient calculation: Application to Central Anatolia. *Earth, Planets and Space*, *63*(8), 903–913. doi: 10.5047/eps.2011.04.003

Ballu, V., Dubois, J., Deplus, C., Diament, M., & Bonvalot, S. (1998). Crustal structure of the Mid-Atlantic Ridge south of the Kane Fracture Zone from seafloor and sea surface gravity data. *Journal of Geophysical Research: Solid Earth*, *103*(B2), 2615–2631. doi: 10.1029/97JB02542

Barthelmes, F. (2009). Definition of functionals of the geopotential and their calculation from spherical harmonic models: theory and formulas used by the calculation service of the International Centre for Global Earth Models (ICGEM), http://icgem. gfz-potsdam. de.
doi: 10.2312/GFZ.b103-09026

Billi, A., Gambini, R., Nicolai, C., & Storti, F. (2007). Neogene-Quaternary intraforeland transpression along a Mesozoic platform-basin margin: The

Gargano fault system, Adria, Italy. *Geosphere*, *3*(1), 1–15. doi: 10.1130/GES00057.1

Blakely, R. J., & Simpson, R. W. (1986). Approximating edges of source bodies from magnetic or gravity anomalies. *Geophysics 51.7*, 1494–1498. doi: 10.1190/1.1442197

Bullard, E. C. (1936). Gravity measurements in east Africa. *Philosophical Transactions of the Royal Society of London. Series A, Mathematical and Physical Sciences*, *235*(757), 445–531.

Ciani, A., Morelli, C., & Gantar, C. (1960). Rilievo gravimetrico sullo zoccolo epicontinentale dei mari italiani. *Boll. Geofis. Teor. Appl*(6), 101p.

Colantoni, P., Tramontana, M., & Tedeschi, R. (1990). Contributo alla conoscenza dell'avampaese apulo: struttura del Golfo di Manfredonia (Adriatico meridionale). *Giornale di Geologia*.

Consortium, E. B., et al. (2018). Emodnet digital bathymetry (dtm 2018).

Corrado, G., et al. (1981). The gravity field of Italy: analysis of its spectral composition and delineation of a tridimensional crustal model for central-southern Italy. *Boll. Geofis. Teor. Appl.*(23), 17–29.

Dawson, G. J., Green, C. M., & Fletcher, K. M. (2015). Using the SAR Mode from CryoSat-2 to Improve Satellite Derived Gravity near the Coast. In *77th eage conference and exhibition 2015* (Vol. 2015, pp. cp–451). doi: 10.3997/2214-4609.201412985

de Alteriis, G. (1995). Different foreland basins in Italy: examples from the central and southern Adriatic Sea. *Tectonophysics*, *252*(1-4), 349–373. doi: 10.1016/0040-1951(95)00155-7

de Alteriis, G., & Aiello, G. (1993). Stratigraphy and tectonics offshore of Puglia (Italy, southern Adriatic Sea). *Marine Geology*, *113*(3-4), 233–253. doi: 10.1016/0025-3227(93)90020-V

Decker, B. L. (1986). *World geodetic system 1984: Defense Mapping Agency Aerospace Center St Louis Afs Mo.*

de Lerma, D., Green, C. M., Cheyney, S., & Campbell, S. J. (2015). Improved high order vertical derivatives of potential field data-extending the ISVD Method. In *77th eage conference and exhibition 2015* (Vol. 2015, pp. 1–5). doi: 10.3997/2214-4609.201412755

Deng, X., & Featherstone, W. E. (2006). A coastal retracking system for satellite radar altimeter waveforms: Application to ERS-2 around Australia. *Journal of Geophysical Research: Oceans*, *111*(C6). doi: 10.1029/2005JC003039

Di Bucci, D., Ravaglia, A., Seno, S., Toscani, G., Fracassi, U., & Valensise, G. (2006). Seismotectonics of the southern Apennines and Adriatic foreland: Insights on active regional E-W shear zones from analogue modeling. *Tectonics*, *25*(4). doi: 10.1029/2005TC001898

Diviacco, P. (2018). *Sismica riconoscitiva legge 613/1967 - zona d.* OGS (Istituto Nazionale di Oceanografia e di Geofisica Sperimentale), Geophysical Section. Retrieved from `https://snap.ogs.trieste.it/cache/service/doi/10.6092/SNAP.580bf950a46873e44295a7e29d66f077` doi: 10.6092/SNAP.580BF950A46873E44295A7E29D66F077

Dubois, J., & Deplus, C. (1989). Gravimetry on the Erimo seamount, Japan. *Tectonophysics*, *160*(1-4), 267–275.

Fairhead, J. D. (2016). *Advances in gravity and magnetic processing and interpretation.* EAGE Publications.

Farr, T. G., & Kobrick, M. (2000). Shuttle Radar Topography Mission produces a wealth of data. *Eos, Transactions American Geophysical Union*, *81*(48), 583–585.

Fedi, M. (2002). Multiscale derivative analysis: A new tool to enhance detection of gravity source boundaries at various scales. *Geophysical Research Letters*, *29*(2), 16–1. doi: 10.1029/2001GL013866

Fedi, M., Cella, F., Florio, G., & Rapolla, A. (2005). Multiscale derivative analysis of the gravity and magnetic fields of Southern Apennines (Italy). *CROP Project, Deep seismic exploration of the Central Mediterranean and Italy (Atlases in Geoscience, Volume 1)", I. Finetti, ed., Elsevier Science*, 281–318.

Fedi, M., & Florio, G. (2001). Detection of potential fields source boundaries by enhanced horizontal derivative method. *Geophysical Prospecting*, *49*(1), 40–58. doi: 10.1046/j.1365-2478.2001.00235.x

Fedi, M., & Rapolla, A. (1993). *I metodi gravimetrico e magnetico nella geofisica della Terra solida.*

Finetti, I. (1983). Struttura ed evoluzione della microplacca adriatica. *Boll. Ocean. Teor. Appl. II (2), 115–123.*

FitzGerald, D., & Milligan, P. (2013). Defining a deep fault network for Australia, using 3D'worming'. *ASEG Extended Abstracts*, *2013*(1), 1–4. doi: 10.1071/ASEG2013ab135

Fu, L.-L., & Cazenave, A. (2000). *Satellite altimetry and earth sciences: a handbook of techniques and applications.* Elsevier.

Fukushima, T. (2019). *Fast computation of prismatic gravitational field.*

Gantar, C. (1983). *Rilievo gravimetrico offshore mgb002: Sullo zoccolo continentale nel mare Adriatico, per l'Agip Mineraria.* Osservatorio Geofisico Sperimentale (OGS), Rel. 5/83 - MNS/1, Rapporto finale N. 82595.

Green, C., Fletcher, K., Cheyney, S., Dawson, G., & Campbell, S. (2019). Satellite gravity – enhancements from new satellites and new altimeter technology. *Geophysical Prospecting*, *67*(6), 1611-1619.

Hildebrand, J. A., Stevenson, J. M., Hammer, P. T. C., Zumberge, M. A., Parker, R. L., Fox, C. G., & Meis, P. J. (1990). A seafloor and sea surface gravity survey of Axial Volcano. *Journal of Geophysical Research: Solid Earth*, *95*(B8), 12751–12763. doi: 10.1029/JB095iB08p12751

Hinze, W. J., Aiken, C., Brozena, J., Coakley, B., Dater, D., Flanagan, G., ... others (2005). New standards for reducing gravity data: The North American gravity database. *Geophysics*, *70*(4), J25–J32. doi: 10.1190/1.1988183

Luyendyk, B. P. (1984). On-bottom gravity profile across the East Pacific Rise crest at 21 north. *Geophysics*, *49*(12), 2166–2177. doi: 10.1190/1.1441632

Mastronuzzi, G., Palmentola, G., & Sansò, P. (2002). Lineamenti e dinamica della costa pugliese. *Studi costieri*, *5*, 9–22.

Miller, H. G., & Singh, V. (1994). Potential field tilt—a new concept for location of potential field sources. *Journal of Applied Geophysics*, *32*(2-3), 213–217. doi: 10.1016/0926-9851(94)90022-1

Morelli, C. (1966). The geophysical situation in italian waters. *The International Hydrographic Review.*

Morelli, D. (2002). Evoluzione tettonico-stratigrafica del Margine Adriatico compreso tra il Promontorio garganico e Brindisi. *Mem. Soc. Geol. It*, *57*, 343–353.

Nagy, D., Papp, G., & Benedek, J. (2000). The gravitational potential and its derivatives for the prism. *Journal of Geodesy*, *74*(7-8), 552–560. doi: 10.1007/s001900000116

Nagy, D., Papp, G., & Benedek, J. (2002). Corrections to" The gravitational potential and its derivatives for the prism". *Journal of Geodesy*, *76*(8), 475–475.

Nowell, D. A. (1999). Gravity terrain corrections—an overview. *Journal of Applied Geophysics*, *42*(2), 117–134. doi: 10.1016/S0926-9851(99)00028-2

Parker, R. L. (1973). The rapid calculation of potential anomalies. *Geophysical Journal International*, *31*(4), 447–455. doi: 10.1111/j.1365-246X.1973.tb06513.x

Pavlis, N. K., Holmes, S. A., Kenyon, S. C., & Factor, J. K. (2012). The development and evaluation of the Earth Gravitational Model 2008 (EGM2008). *Journal of Geophysical Research: Solid Earth*, *117*(B4). doi: 10.1029/

2011JB008916

Rapolla, A. (1986). Crustal structure of Central and Southern Italy from gravity and magnetic data. *Giornale di Geologia*, *48*(1-2), 129–143.

Ridente, D., Fracassi, U., Di Bucci, D., Trincardi, F., & Valensise, G. (2008). Middle Pleistocene to Holocene activity of the Gondola Fault Zone (Southern Adriatic Foreland): Deformation of a regional shear zone and seismotectonic implications. *Tectonophysics*, *453*(1-4), 110–121. doi: 10.1016/j.tecto.2007.05.009

Ridente, D., & Trincardi, F. (2006). Active foreland deformation evidenced by shallow folds and faults affecting late Quaternary shelf–slope deposits (Adriatic Sea, Italy). *Basin Research*, *18*(2), 171–188. doi: 10.1111/j.1365-2117.2006.00289.x

Sandwell, D. T. (1992). Antarctic marine gravity field from high-density satellite altimetry. *Geophysical Journal International*, *109*(2), 437–448. doi: 10.1111/j.1365-246X.1992.tb00106.x

Sandwell, D. T., Garcia, E., Soofi, K., Wessel, P., Chandler, M., & Smith, W. H. F. (2013). Toward 1-mGal accuracy in global marine gravity from CryoSat-2, Envisat, and Jason-1. *The Leading Edge*, *32*(8), 892–899. doi: 10.1190/tle32080892.1

Sandwell, D. T., Müller, R. D., Smith, W. H. F., Garcia, E., & Francis, R. (2014). New global marine gravity model from CryoSat-2 and Jason-1 reveals buried tectonic structure. *Science (New York, N.Y.)*, *346*(6205), 65–67. doi: 10.1126/science.1258213

Sandwell, D. T., & Smith, W. H. (2009). Global marine gravity form retracked Geosat and ERS-1 altimetry: Ridge segmentation versus spreading rate. *Journal of Geophysical Reseach*, *10*. doi: 10.1029/2008JB006008

Stacey, F. D., & Tuck, G. J. (1981). Geophysical evidence for non-Newtonian gravity. *Nature*, *292*(5820), 230–232. doi: 10.1038/292230a0

Talwani, M., Early, W. P., & Hayes, D. E. (1966). Continuous analog computation and recording of cross-coupling and off-leveling errors. *Journal of Geophysical Research*, *71*(8), 2079–2090. doi: 10.1029/JZ071i008p02079

Tramontana, M., Morelli, D., & Colandoni, P. (1995). Tettonica plio-quaternaria del sistema sud-garganico (settore orientale) nel quadro evolutivo dell'Adriatico centro-meridionale. *Studi geologici camerti, n. speciale, 1995, pp. 467-473*.

Uieda, L., Soler, S. R., Pesce, A., Oliveira Jr, V. C., & Shea, N. (2020). Harmonica: Forward modeling, inversion, and processing gravity and magnetic data (Version v0.1.0). doi: 10.5281/zenodo.3628742

Volpi, V., Forlin, E., Baroni, A., Estublier, A., Donda, F., Civile, D., ... Delprat-Jannaud, F. (2015). Evaluation and Characterization of a Potential CO2 Storage Site in the South Adriatic Offshore. *Oil & Gas Science and Technology–Revue d'IFP Energies nouvelles*, *70*(4), 695–712. doi: 10.2516/ogst/2015011

Wessel, P., Luis, J. F., Uieda, L., Scharroo, R., Wobbe, F., Smith, W. H., & Tian, D. (2019). The generic mapping tools version 6. *Geochemistry, Geophysics, Geosystems*, *20*(11), 5556–5564. doi: 10.1029/2019GC008515

Wijns, C., Perez, C., & Kowalczyk, P. (2005). Theta map: Edge detection in magnetic data. *Geophysics*, *70*(4), L39–L43. doi: 10.1190/1.1988184

Table 1. Statistics of differences between sea-bottom gravity datasets OGS60 and OGS83 (see, Figure 4)

	Min	**Max**	**Min**	**Std**	**RMS**
OGS83-OGS60	-0.79	1.7	0.1	0.57	0.58

Unit of measure in mGal

Table 2. Statistic of Bouguer gravity anomaly calculated for each dataset (DTU, OGS and S&S) and relative differences within a 17 km wide coastal strip (DTU-S&S, DTU-OGS, DTU-OGS).

	Min	**Max**	**Min**	**Std**	**RMS**
DTU	41.04	124.49	64.18	11.73	-
S&S	41.78	123.87	66.46	12.01	-
OGS	42.13	102.24	60.6	6.52	-
DTU-S&S	-27.44	8.5	-3	6.34	7.01
DTU-OGS	-20.47	19.18	1.11	4.03	4.18
S&S-OGS	-7.43	38.57	4.11	6.78	7.93

Unit of measure in mGal

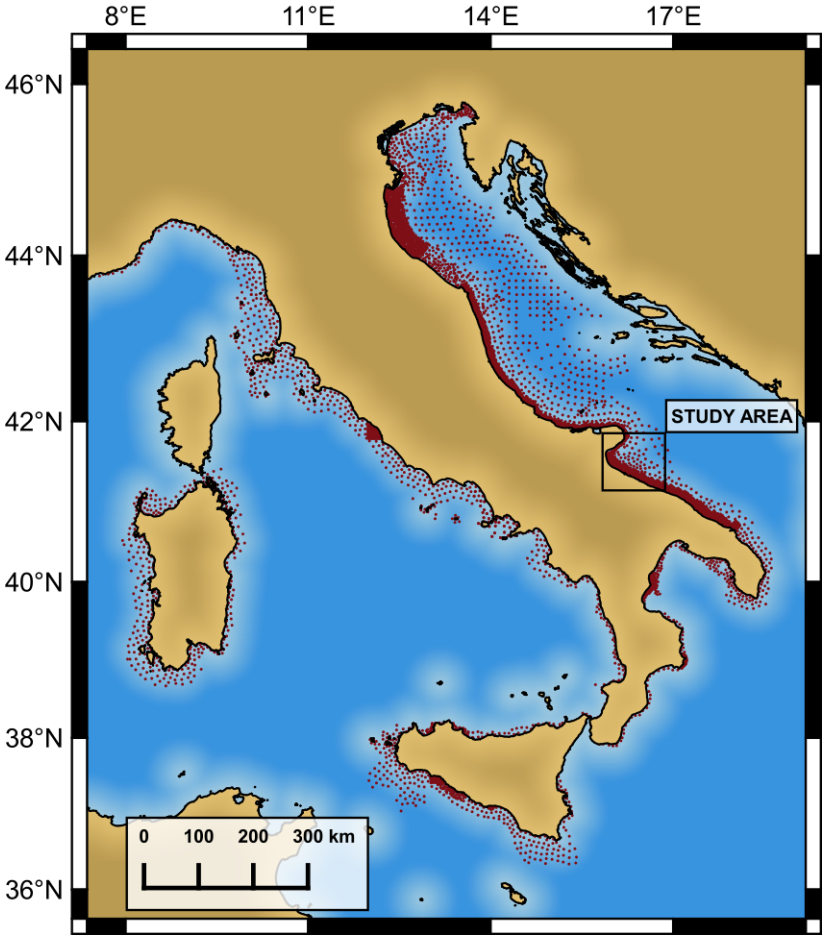

Figure 1. Position of sea-bottom gravity stations (small red dots) from the OGS database, including C. Morelli (1966) and Gantar (1983). Most of the stations have been recorded from the early 50's to the late 80's, a few tens of kilometres from the Italian coasts, with an average spacing of about 1 km. Map frame in WGS84 World-Mercator coordinate system (EPSG: 6893).

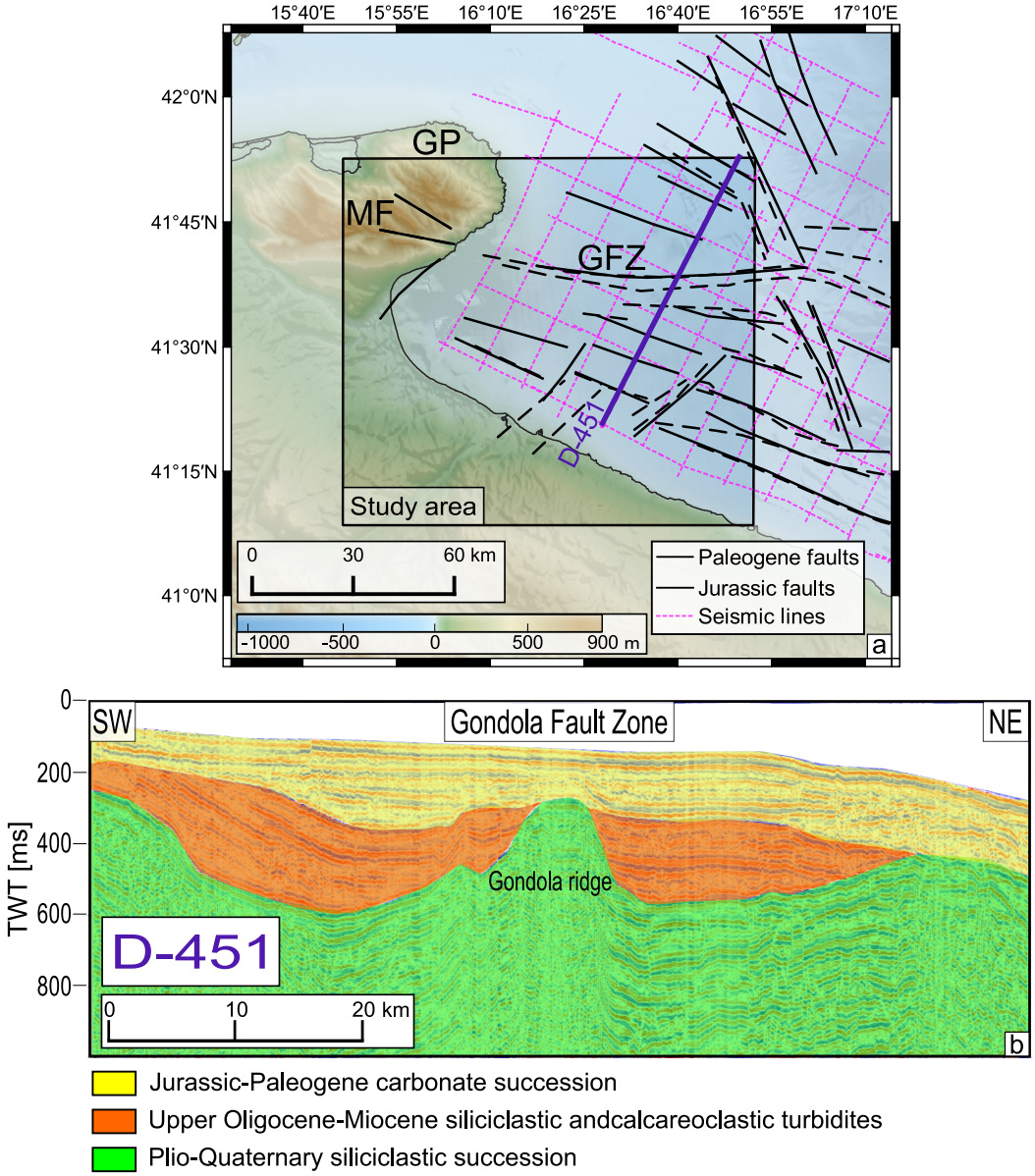

Figure 2. (a) Structural map of the Gulf of Manfredonia, showing the Gondola Fault Zone (GFZ) and its inland continuation with the Mattinata Fault (MF) cutting through the Gargano Promontory (GP). Fault interpretation in the marine sector has been derived from seismic data (D. Morelli, 2002), and position of the multichannel seismic profiles from ViDEPI (violet lines). (b) Seismic profile D-451 (position in Figure 2a), where the Gondola ridge is clearly imaged (interpretation of seismic layers has been taken from Volpi et al. (2015)). Seismic data comes from the project ViDEPI "Visibility of Petroleum Exploration Data in Italy" (URL: www.videpi.com), managed by the Ministry of Economic Development. Data have been made available in the SEG-Y on the platform SNAP "Seismic data Network Access Point", managed by the Istituto Nazionale di Oceanografia e di Geofisica Sperimentale, OGS (Diviacco, 2018).

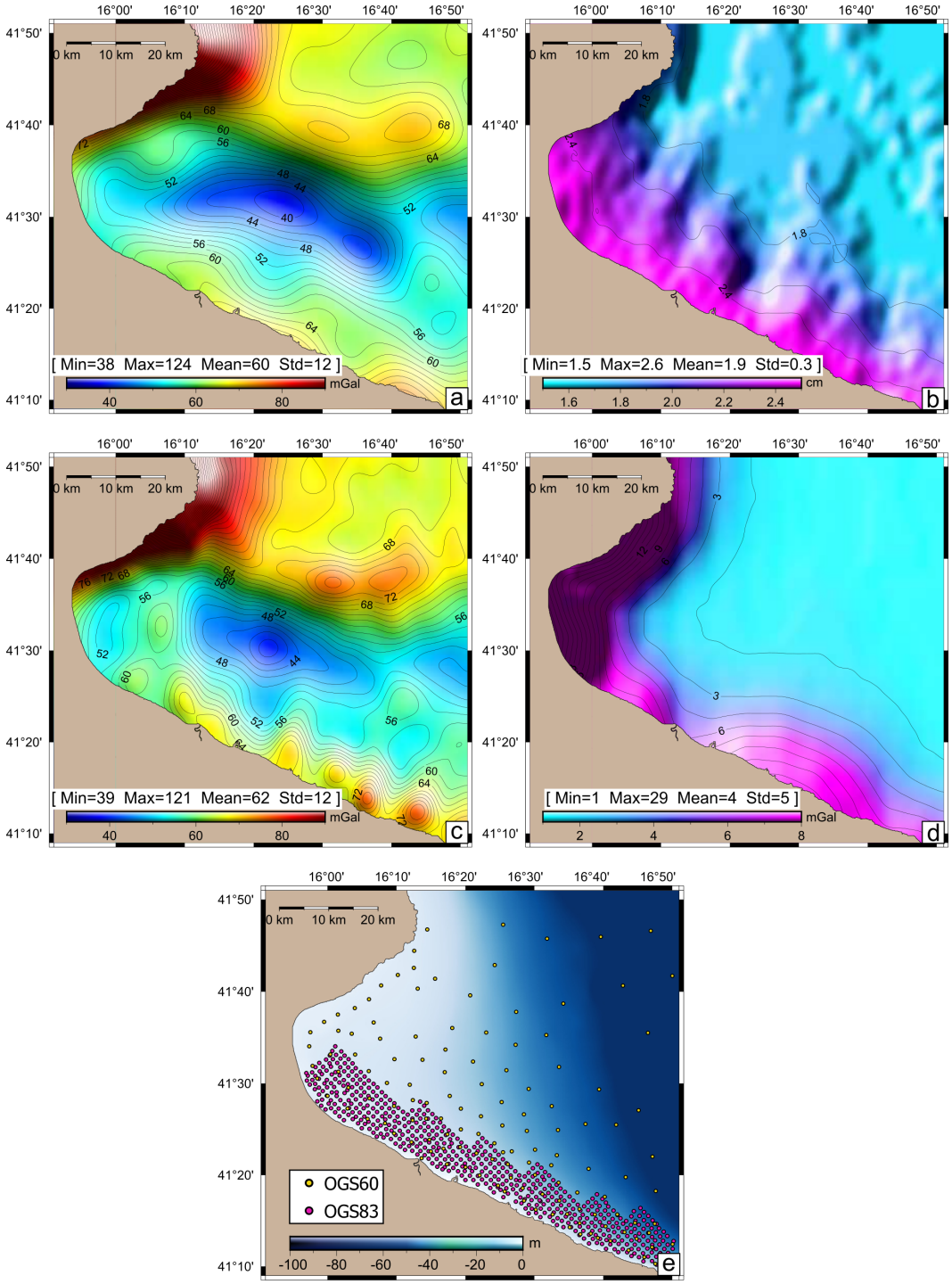

Figure 3. Free air anomaly of DTU dataset with associated MSS interpolation error (a,b) and Free-air anomaly of S&S dataset with associated RMS error (c,d). The interpolation error of DTU is given in metric units (cm) which can be roughly converted into mGals using the constant ratio of ∼1.4 mGal/cm. Instead, the RMS error of S&S is directly given in mGal units. The error maps show how the quality of the Free-air anomaly deteriorates near the coast, up to a maximum of 29 mGal in S&S data. The lowest map (e) show the position of sea-bottom gravity stations, plotted onto the Gulf of Manfredonia bathymetry: OGS 1960 (yellow dots) and OGS 1983 (red dots).

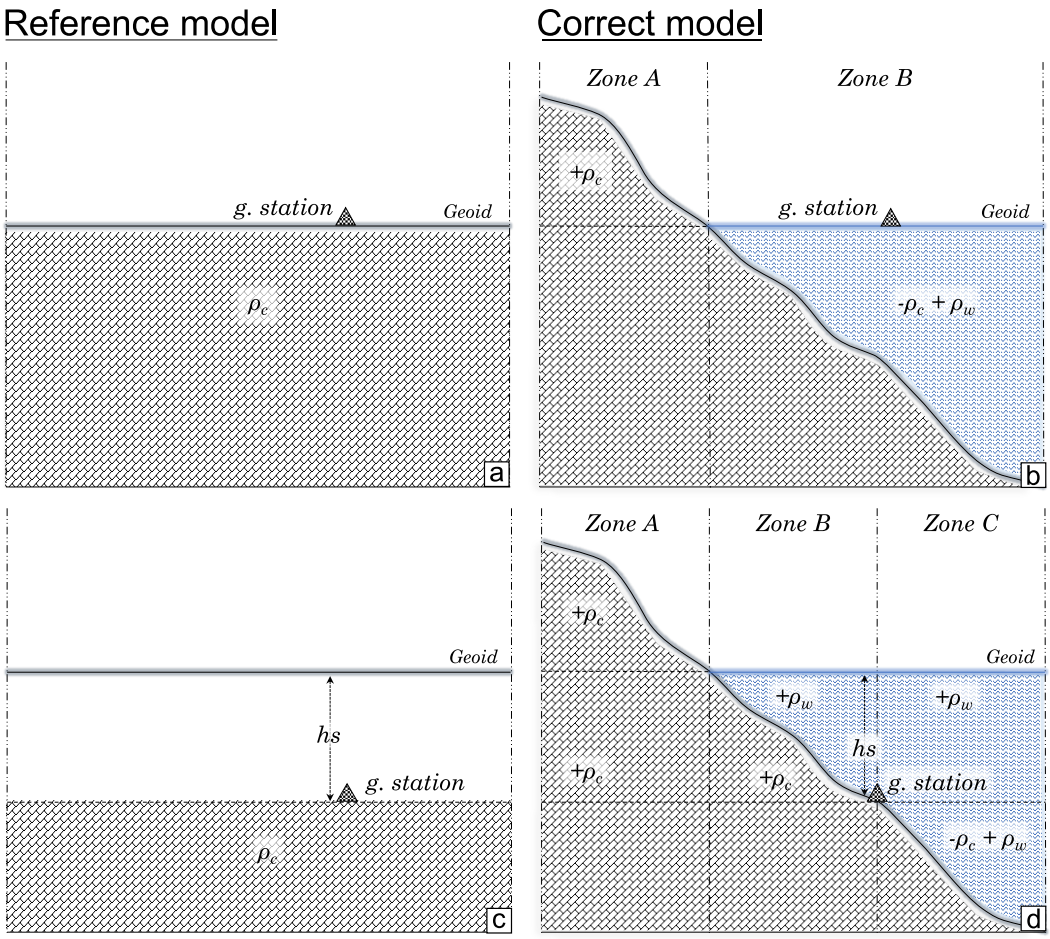

Figure 4. Schematic representation of models used to compute topographic effects of sea surface gravity (a, b, eq. 10) and sea bottom gravity (c, d, eq. 11). On the left, the reference model, and on the right, the correct model including all the density corrections that must be added to the reference model in order to have a correct estimate of the topographic effect.

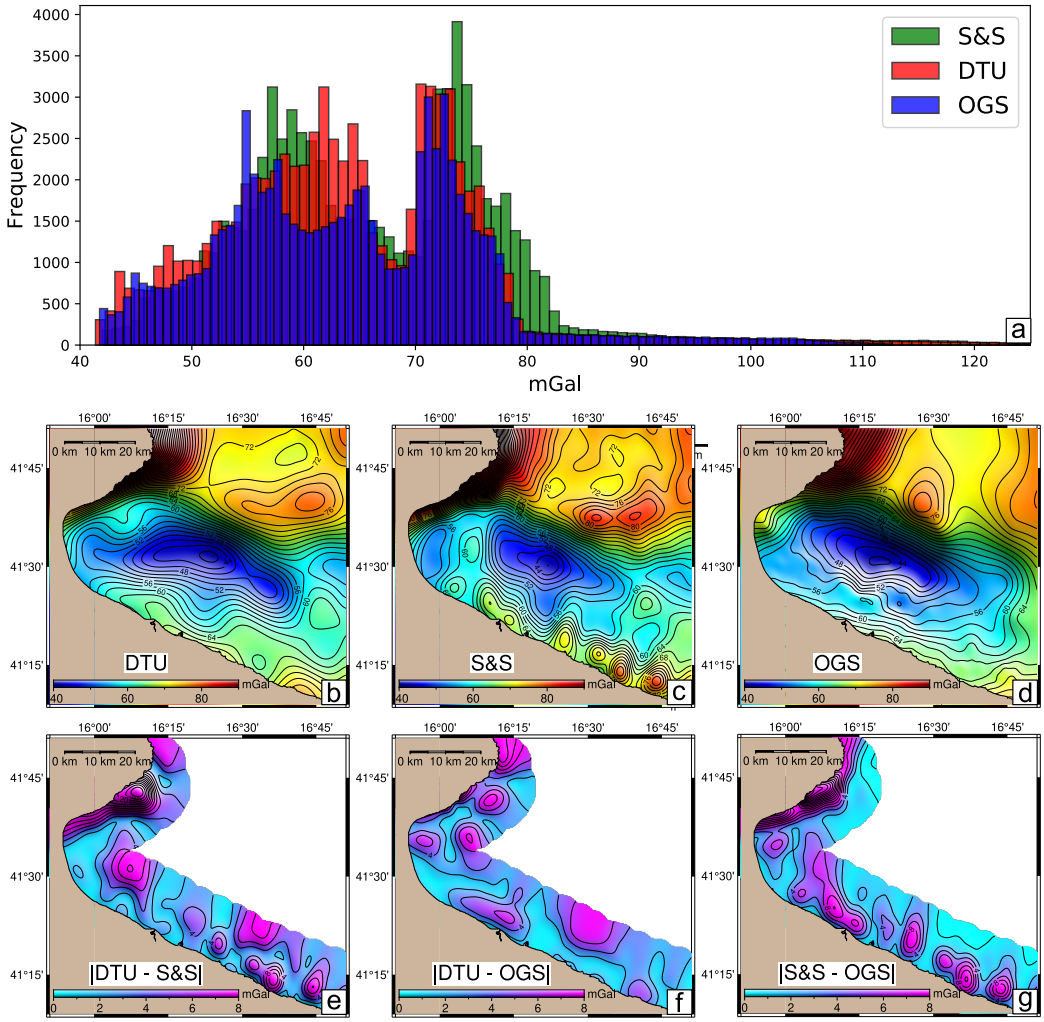

Figure 5. Distribution of Bouguer anomaly values (a), Bouguer anomaly maps (b, c, d) and relative absolute differences of DTU, S&S, OGS datasets (e, f, g). A block mean average, with ∼2 km window size, and low-pass gaussian filter, with a 6 km window size, have been used (i) to avoid aliasing errors (Wessel et al., 2019), and (ii) to bring all dataset to the same empirical lowest resolution. The differences are mapped within a 15 km wide coastal strip, which is the area mostly affected by coastal noise in satellite data and, at the same time, densely covered by the OGS sea-bottom stations. The absolute value stresses the total magnitude of differences, without the bias of the sign. The coastal noise is easy to identify in the S&S dataset and in the S&S-OGS differences, where it forms a sort of "ringing effect" up to ∼17 km seaward.

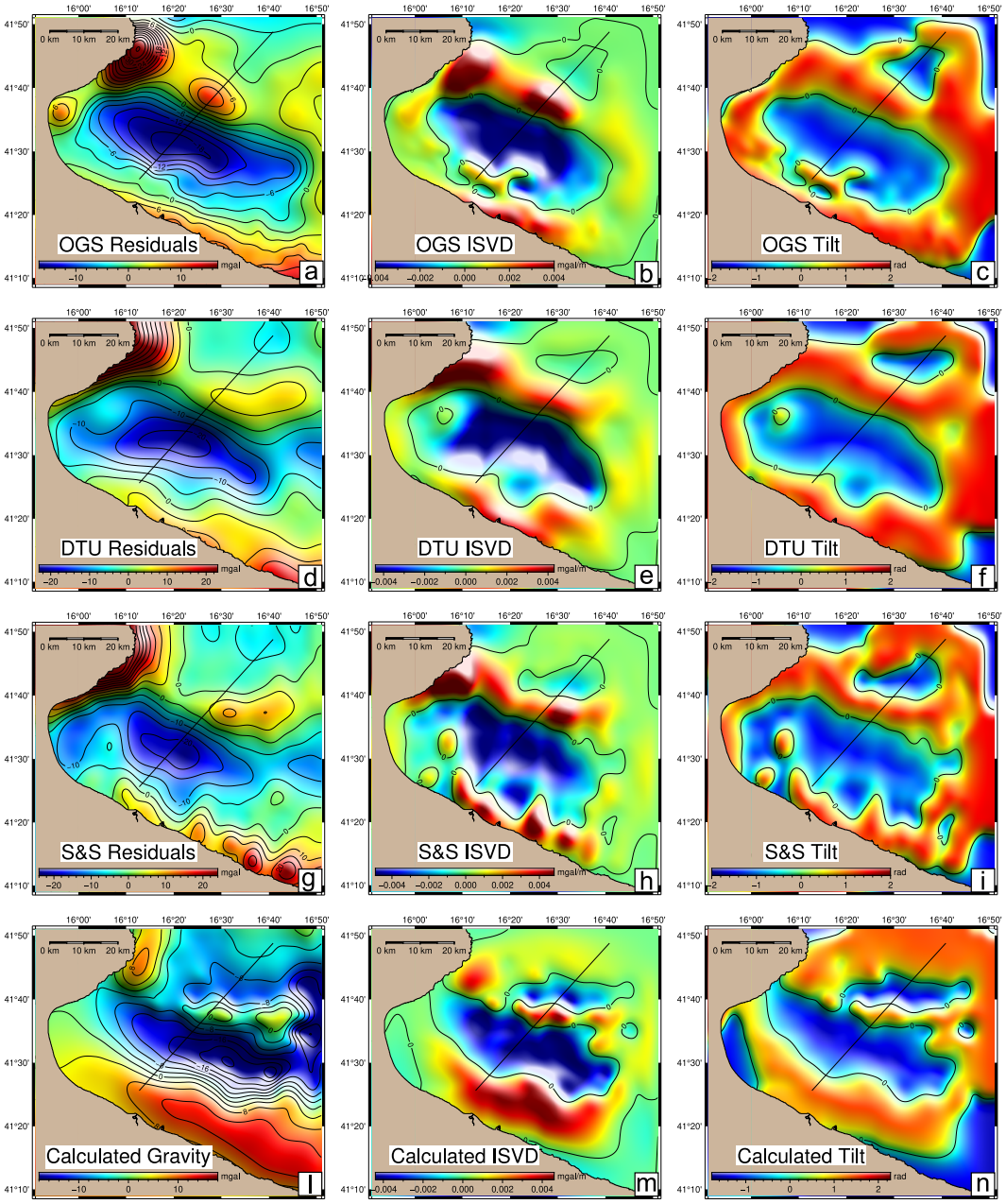

Figure 6. The subplots show from left to right, (i) the observed gravity residuals, (ii) the Integrated Second Vertical Derivative (ISVD) and (iii) the Tilt function of DTU (a,b,c), S&S (d,e,f) and OGS (g,h,i) datasets. The bottom plots (l,m,n) show the calculated gravity effect of the 2-D depth-interface, obtained from seismic reflection data depth converted, which separates sedimentary deposits from carbonate rocks. Black line indicates the profile analysed in figure 7.

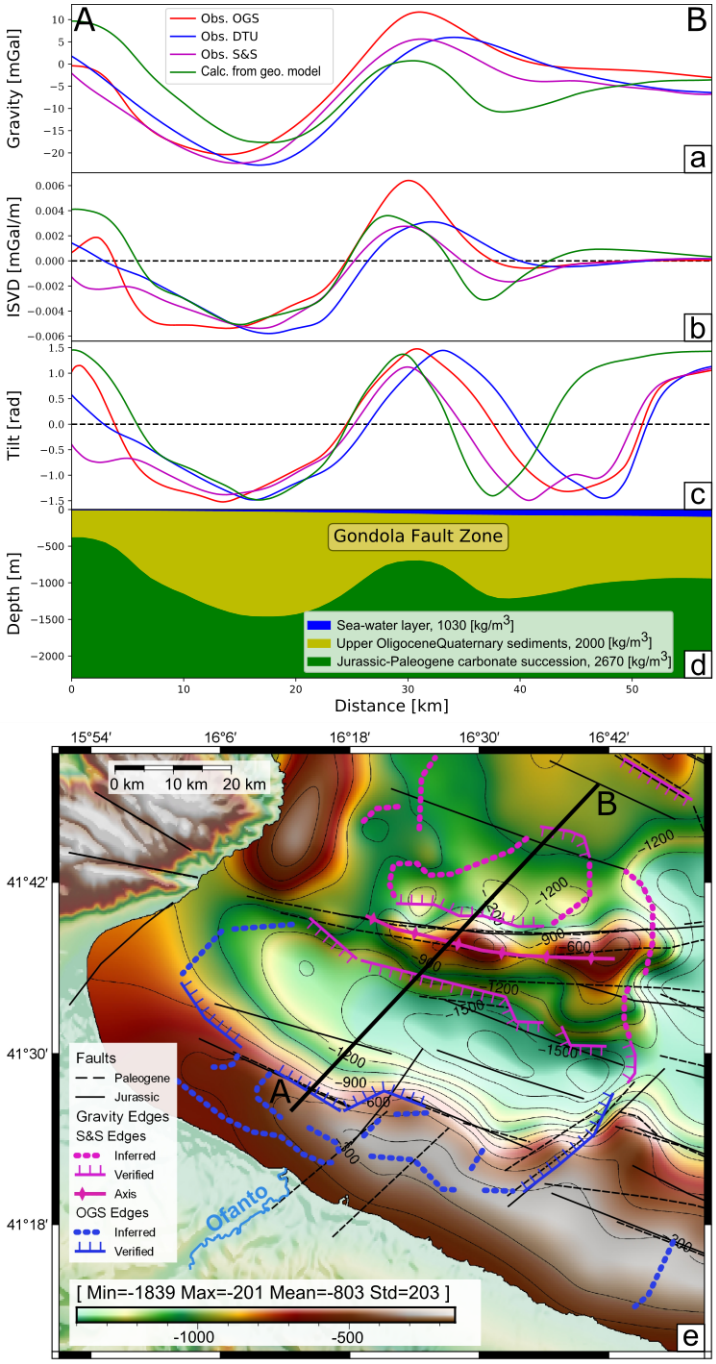

Figure 7. Representative depth profile of the geological model derived from seismic interpretation, crossing the Gondola Fault Zone (d). Upper panels (a, b, c) show the trend of the observed residual gravity, ISVD, and Tilt functions, calculated for each different dataset (OGS, DTU, and S&S), and for the geological model. The zero values of both ISDV and Tilt approximately marks the upper edges of the carbonate platforms. The bottom map (e) show with results from the edge-detection analysis, which combines OGS data up to 17 km from the coast and S&S data in the remaining areas. The gravity-edges have been divided in two sets: the first set contains lines correlating with the general trend of the faults (verified edges), and the second set contains lines only recorded by gravity (inferred edges). The ridge axis outline approximately the top-centre of the Gondola ridge. The rock/sediment interface is imaged and contoured onto the off shore areas (Volpi et al., 2015). Jurassic-Paleogene faults are both based on seismic interpretations taken from previous works (D. Morelli (2002), and references therein).